Dalton Transactions

Cite this: *Dalton Trans.*, 2012, **41**, 10941

www.rsc.org/dalton

PAPER

Thorium nanochemistry: the solution structure of the Th(IV)–hydroxo pentamer†

Clemens Walther,‡ Jörg Rothe,* Bernd Schimmelpfennig and Markus Fuss

Received 2nd February 2012, Accepted 10th April 2012
DOI: 10.1039/c2dt30243h

Tetravalent thorium exhibits a strong tendency towards hydrolysis and subsequent polymerization. Polymeric species play a crucial role in understanding thorium solution chemistry, since their presence causes apparent solubility several orders of magnitude higher than predicted by thermodynamic data bases. Although electrospray mass spectrometry (ESI MS) identifies Th(IV) dimers and pentamers unequivocally as dominant species close to the solubility limit, the molecular structure of $Th_5(OH)_y$ polymers was hitherto unknown. In the present study, X-ray absorption fine structure (XAFS) spectroscopy, high energy X-ray scattering (HEXS) measurements, and quantum chemical calculations are combined to solve the pentamer structure. The most favourable structure is represented by two Th(IV) dimers linked by a central Th(IV) cation through hydroxide bridges.

Introduction

Hydrolysis reactions play an important role in the aqueous solution chemistry of dissolved metal ions.[1] Although they have been known for some time, a molecular-level understanding of subsequent metal-ion condensation to form polynuclear clusters remains elusive. It is well known that hydrolysis reactions are favoured with increasing hardness and concentration of the dissolved metal ion and with increasing solution pH. In contrast to tetravalent plutonium which was shown to form very inert oxygen bridged clusters,[2] the softest tetravalent ion in the periodic table, Th, forms mostly hydroxide bridged polymers and holds a special role in unraveling the complex chemistry associated with these hydrolysis reactions. A number of recent studies have focused on Th at rather high concentrations in acidic media such as hydrochloric acid, nitrate[3] and perchloric acid.[4] Even at moderate pH thorium hydrolyses rather quickly,[5] which in turn leads to formation of polynuclear hydroxide complexes and colloids.[6] These species play a crucial role in understanding thorium solution chemistry, since their presence causes apparent solubilities several orders of magnitude higher than in the absence of polymerization.[7] Furthermore, reactivity and extractability of polymeric species differ a lot from monomers due to their high charge. It is hence necessary to understand formation of polymers quantitatively on a molecular level.

Most information on the presence of polymers is gained from indirect methods such as coulometric titration which require a model and well defined starting conditions (*e.g.*, the presence of 100% of one known species at the starting point of the titration). Methods aiming at structural investigations very often require samples which contain only one polymeric species and are applicable only at very high concentrations. Recently, we reported on a direct way of detecting metal hydroxide complexes by electrospray mass spectrometry (ESI MS).[8–10] This technique allows us to quantify many species simultaneously, down to less than 1% contribution to the total metal content[11] (details on the technique are reported in ref. 12). The number of metal ions, ligand molecules and the charge of the complex are measured independently, which is equivalent to the determination of the stoichiometry of the solution species. ESI MS was first applied to thorium in solution by Moulin *et al.*[13] At the high acidity and the rather harsh declustering conditions used in this study only monomeric complexes were found. Using much milder conditions[11,14] allowed us to identify dimers and pentamers which are the dominant polymeric complexes close to the solubility limit. Based on these findings we proposed an alternative description of Th-solubility including a stepwise quasi-continuous hydrolysis of polymers. However, though the species were identified unequivocally, we could not tell anything about their structure. To this end we combined X-ray absorption fine structure (XAFS), high energy X-ray scattering (HEXS) measurements, and quantum chemical calculations in the present work.

Experimental

Sample preparation

Samples of six different concentrations ranging from $[Th]_{tot}$ = 0.12 M (series **A**) through $[Th]_{tot} = 2 \times 10^{-4}$ M (series **F**) were

Institut für Nukleare Entsorgung, Karlsruhe Institute of Technology (KIT-INE), P.O. Box 3640, D-76021 Karlsruhe, Germany. E-mail: rothe@kit.edu

†Electronic supplementary information (ESI) available: see DOI: 10.1039/c2dt30243h

‡Present address: Institut für Radioökologie und Strahlenschutz, Leibniz Universität Hannover, Herrenhäuser Str. 2, D-30419 Hannover, Germany.

Table 1 Species distribution according to ESI MS measurements as a function of total thorium concentration, pH_C, and age

			Age (days)		Complex (x,y): $Th_x(OH^-)_y^{4x-y}$/% of $[Th]_{tot}$							
	$[Th]_{tot}$ (M)	pH_C	ESI	XAFS	(1,0)	(1,1)	(1,2)	(1,3)	(2,*y*)	$\bar{y}$	(5,*y*)	$\bar{y}$
A1	1.3×10^{-1}	1.1	0	1	53	42	3	2	—	—	—	—
	1.3×10^{-1}	1.1	90		44	44	8	4	—	—	—	—
A2	1.0×10^{-1}	2.1	0	1	40	42	3	2	13	1.0	—	—
	1.0×10^{-1}	2.1	90		32	50	13	3	12	1.5	—	—
A3	9.8×10^{-2}	2.93	0	1	7	16	12	2	28	3.7	35	12.7
	9.8×10^{-2}	2.93	90		1	18	20	11	37	4.4	13	12.4
	9.8×10^{-2}	2.93	287		29	24	11	4	14	4.0	18	12.0
A4	1.2×10^{-1}	3.03	0		4	15	13	4	24	3.9	40	13.9
	1.2×10^{-1}	3.03	287		3	10	8	2	24	6.0	53	13.1
A5	1.1×10^{-1}	3.04	0		3	14	8	2	24	4.0	49	13.1
A6	1.2×10^{-1}	3.05	0		4	12	8	3	23	4.0	50	13.8
A7	1.2×10^{-1}	3.05	0	1	1	11	9	4	31	4.0	44	14.2
	1.2×10^{-1}	3.05	287		5	11	9	3	21	6.0	51	12.6
A8	1.2×10^{-1}	3.05	0		0.3	4	3	0.7	8	4.1	84	13.7
	1.2×10^{-1}	3.05	90		2	11	6	2	21	4.0	58	13.1
	1.2×10^{-1}	3.05	419		2	9	5	2	17	4.0	65	13.3
A9	8.9×10^{-2}	2.88	1		2	21	13	2	28	6.0	34	13.5
A10	8.9×10^{-2}	2.88	2		3	22	11	3	27	6.0	34	13.0
A11	9.0×10^{-2}	3.05	1		2	22	12	4	25	6.0	35	13.6
A12	9.0×10^{-2}	3.05	2		3	17	8	1	20	6.0	51	15.0
B1	1.6×10^{-2}	3.46	0	1	0.3	10	7	2	—	—	81	15.3
B2	1.7×10^{-2}	3.49	0		0.5	7	6	1	0.5	6.0	85	14.2
B3	1.6×10^{-2}	3.56	0		2	18	11	3	1	6.0	65	15.7
C1	1.6×10^{-3}	3.55	0	1	2	22	10	3	—	—	63	15.7
C2	1.6×10^{-3}	3.75	0		2	23	11	3	—	—	61	15.8
D1	6.9×10^{-4}	3.67	4		8	36	15	5	—	—	36	14.5
D2	6.8×10^{-4}	3.67	0	1	4	30	17	5	—	—	44	14.5
E1	3.4×10^{-4}	3.86	1	1	1	30	10	7	1	6.0	51	15.8
F1	2.7×10^{-4}	3.83	1	1	9	47	16	4	—	—	24	16.3

prepared by further diluting a stock solution ($[Th]_{tot}$ = 0.35 M, pH 2.3) of redissolved $Th(OH)_4$ with HCl of appropriate concentration as described in ref. 11. For each Th concentration, the pH of the samples was chosen close to the solubility curve of amorphous Th hydroxide which decreases by the third power of H^+ concentration[7] (Table 1) (Fig. 1).

Quantum chemical calculations

All calculations were carried out with the TURBOMOLE program package.[15] For the initial gas-phase geometry optimization we employed the RI-DFT[16–18] approach with the BP86 functional[19–23] using for Th the small-core pseudo-potential (PP) of Stuttgart–Cologne type in combination with a segmented basis set (14s13p10d8f)/[10s9p5d4f] by Cao *et al.*[24,25] augmented by one *g*-function (α = 0.32) as well as basis sets of TZVP quality on oxygen and hydrogen. PP, basis sets as well as auxiliary basis sets were provided by the TURBOMOLE libraries. Scalar relativistic effects on the heavy center are included in the PP, whereas spin–orbit effects would be of second order for all closed-shell complexes under investigation and were therefore negligible.

XAFS measurements

Selected samples (indicated in Table 1) were measured by room temperature Th L3-XAFS spectroscopy at the Ångströmquelle Karlsruhe (ANKA), KIT North Campus, at the INE-Beamline for actinide research.[26] The spectra were calibrated against the first inflection point in the XANES of Y metal (assigned as

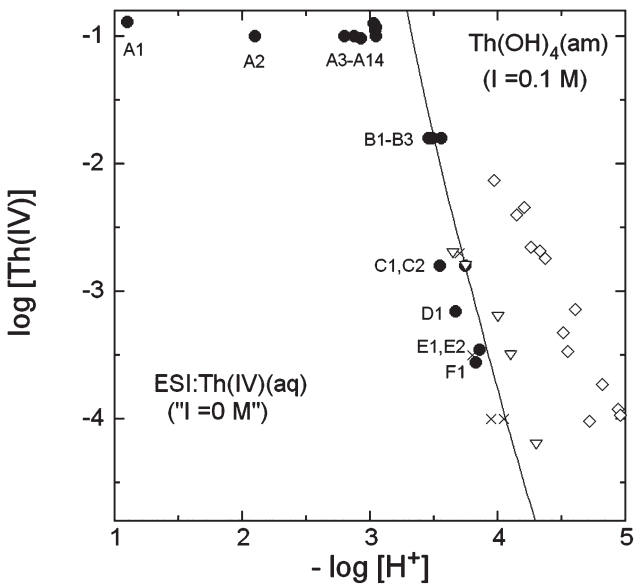

Fig. 1 Solubility diagram for $Th(OH)_4$(am). Samples measured by ESI (•, *cf.* Table 1). Solid line: solubility calculated for Th(IV) in HCl without addition of electrolytes (I = 0). Formation constants and SIT parameters from ref. 7. Open symbols represent experimental solubility data at I = 0.1 M from Nabivanets *et al.*[39] (▽), Ryan *et al.*[40] (×), and Rai *et al.*[41] (◇).

17 038 eV, *i.e.*, the Y 1s energy). For samples with metal concentrations >10 mM the transmission signal recorded with Ar-filled ionization chambers at ambient pressure was analyzed. Samples with lower concentrations were measured in fluorescence detection mode by registering the Th $L\alpha_{1,2}$ fluorescence yield at ~12 900 eV using a five-pixel Ge solid state detector (Canberra LEGe). Up to 8 scans were collected at room temperature and averaged for each sample. EXAFS data analysis (*cf.* ref. 12 and references therein) was based on standard techniques using the ATHENA (v0.8.050) and the UWXAFS software packages. E_0, the origin used to calculate the EXAFS $\chi(k)$ function, was fixed at the white line (WL) maximum position of the Th L3-XANES. EXAFS fit parameters (neighboring atom distances R_i, EXAFS Debye–Waller factors $\sigma^2{}_i$ and coordination numbers N_i for coordination shell i) were determined using the feffit code (v2.98). Backscattering amplitude and phase shift functions for single scattering paths were calculated for a 45-atom ThO_2 cluster with fluorite structure using FEFF8.2. Prior to analysis, the k^3-weighted Th L3-EXAFS was Fourier-transformed over a k-space range of ~2.5–15.5 $Å^{-1}$, using symmetric square windows with Δk = 0.2 $Å^{-1}$ 'Hanning sills'. All fit operations were performed in R-space. The amplitude reduction factor $S_0{}^2$ was fixed at 1.0.

HEXS

The data were collected at the Advanced Photon Source, Sector 11-ID-B, operating at 91 keV, using a GE Healthcare, amorphous-Si detector over a momentum transfer range of 0.3 to 35 $Å^{-1}$. After subtracting scattering patterns from blank solutions and the sample holder, the data were Fourier transformed to provide a pair distribution function (PDF).

Results and discussion

ESI MS measurements revealed two major trends (Table 1): at low pH monomers prevail (**A1** at pH 1.1) and a rather small fraction of dimers is formed at pH 2.1 (**A2**). Between pH 2.9 and 3.15, *i.e.*, close to the point of precipitation and formation of amorphous $Th(OH)_4$ (in the following denominated solubility limit), larger polymers exist, in particular the pentamers $Th_5(OH)_y$. Several pentamers with different numbers of hydroxide ligands are present simultaneously (typically $12 < y < 17$) and their mean values ($\bar{y}$) increase as a function of pH (*cf.* ref. 11). This effect is independent of $[Th]_{tot}$, in analogy to the case of monomeric hydroxide complexes. Over a time period of up to one year the pentamers are stable 'steady state' species, though we cannot be certain that the solutions reached thermodynamic equilibrium since there is evidence that kinetics might be very slow in the case of Th solids.[27] In slightly oversaturated solutions Ostwald ripening leads to formation of nm-sized colloids at the expense of polymers.[14] The second important finding is that the relative abundance of polymers, *i.e.*, the percentage of Th^{4+} ions contained in a size fraction, is not so much a function of absolute Th concentration but rather a function of the degree of saturation. In other words, even low concentrated samples may contain a high fraction of polymers as the solubility limit is approached: the maximum contribution of pentamers (~85%) was achieved not only for the most concentrated solutions of series **A** but also at tenfold lower $[Th]_{tot}$ in the case of sample **B2**. At $[Th]_{tot}$ < 1 mM pentamers still contribute >50% (series **E**), which is in accordance with the findings of Neck *et al.* that at neutral pH and $[Th]_{tot} < 10^{-6}$ M, Th polymers or colloids contribute >90% of 'suspended' thorium.[6] These findings stress the relevance of Th-polymers even at low concentration.

Th L3-XAFS spectra taken from fresh samples (*i.e.*, within one day after preparation) were free of characteristic particle size effects generally observed for nm-sized colloids (*i.e.*, WL dampening and broadening[28]). Hence, metal–metal distances detected by XAFS have to be attributed to the existence of polymeric species. At $[Th(IV)]_{tot}$ = 0.68 mM and pH_C 3.67, (**D2**) 44% of the Th species are found to be (5,15)-pentamers ((*x*,*y*) denotes the $Th_x(OH^-)_y{}^{4x-y}$ complex, *cf.* Table 1) according to ESI MS, while 56% are monomers. Two coordination shells are discernible in the EXAFS FT. Note that the feature generally visible at ~1.4 Å ($R - \Delta$) in the FT of Th L3-XAFS data is most probably due to atomic contributions or to multielectron excitations in the EXAFS regime.[29,30] Hence, it is not reproduced by the curve fitting and leads to a slight mismatch between the experimental and Fourier-filtered data in k-space (Fig. 2, right panel). The dominant FT peak around 1.9 Å ($R - \Delta$) reflects Th bonding to bridging and terminal hydroxide groups and to oxygen from terminal water. The Th–O distance spread requires two oxygen shells in the fit. The shorter distance (3.8 O at 2.40 Å) is attributed to bridging and terminal OH^- groups, and the longer (3.4 O at 2.55 Å) to terminal water. The average oxygen coordination number (7–8) is significantly reduced compared to the aquo ion (10 O at 2.45 Å[31]). Assuming an average of 8 oxygen neighbors for each Th atom in the pentamer, one would expect a somewhat larger value of 9–10. The well resolved second shell around 3.7 Å ($R - \Delta$) reflects backscattering from Th neighbors in the pentamers. Only one Th–Th distance is discernible from the data. The fit yields 1.7 Th at 3.87 Å, which is in accordance with the assumption of Th having 2.4 second next Th neighbors in the pentamer and none such in the monomer. N_{Th} is found to be slightly increased for sample **C1** ($[Th(IV)]_{tot}$ = 1.6 mM, pH_C 3.55, 63% pentamers), as expected due to the increased percentage of pentamers. The apparent increase of the Th–Th distance (3.87 Å *vs.* 3.94 Å) might be due to a larger bonding asymmetry of the pentamers present in sample **D2**.[32] Fit results for sample **B1** at $[Th(IV)]_{tot}$ = 16 mM are shown in Fig. 3, top row. For this sample (pH_C 3.46, 81% pentamers) we observed a significant increase of N_{Th} (3.1 Th at 3.94 Å), reflecting the increasing polymerization at this concentration range. The Th–O coordination (8.8 O at 2.49 Å – no splitting, but a larger Debye–Waller factor of 0.013 $Å^2$) is in full accordance with assumption of the average contribution of N_O = 10 for 20% monomers and N_O ~ 8 for 80% pentamers to the EXAFS. Upon further increase of $[Th(IV)]_{tot}$ the aforementioned fact that the degree of polymerization primarily depends on the oversaturation at a given pH_C becomes obvious: at $[Th(IV)]_{tot}$ = 131 mM, pH_C 1.1, sample **A1** and 100 mM, pH_C 2.1, sample **A2**, respectively, no Th–Th interaction is discernible from the XAFS. The large amplitude and single sinusoidal behavior of the $\chi(k)$ function (Fig. 2, middle row) reflects the dominant presence of Th(IV) monomers in agreement with ESI MS results (100% for sample **A1** and 87% for sample **A2**) with around nine oxygen atoms coordinated at 2.45–2.47 Å. When

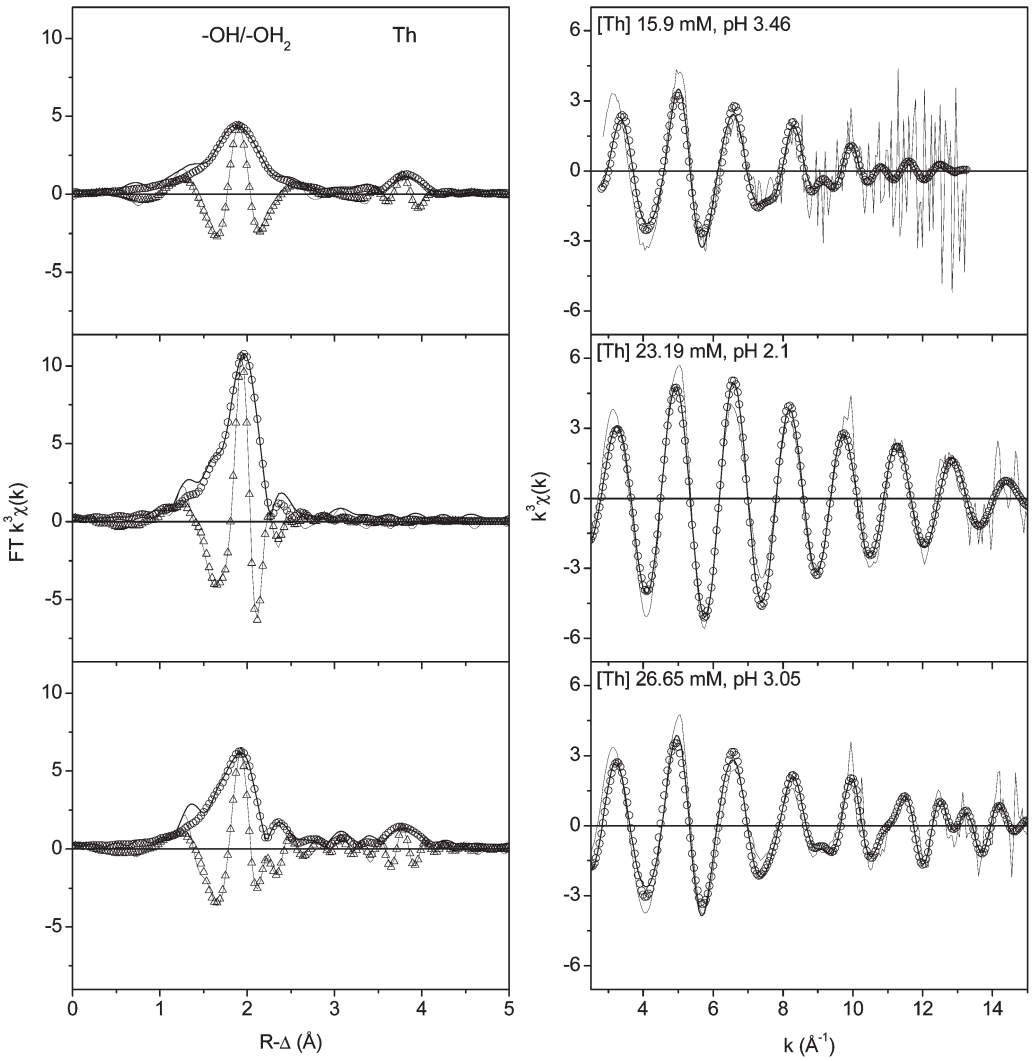

Fig. 2 Th L3-EXAFS *R*-space fit results for samples **B1**, **A2** and **A7**. Left panel: FT magnitude of EXAFS data (solid line), fit magnitude (open circles), FT real part (thin solid line) and fit real part (open triangles). Right panel: corresponding Fourier-filtered data (solid line), back-transformed fit (open circles) and k^3-weighted experimental data (thin solid line).

approaching the Th(IV) solubility threshold a second shell Th backscattering path is again detectable for sample **A3** ($[Th(IV)]_{tot}$ = 98 mM, pH_C 2.93, 35% pentamers) and increasingly visible for sample **A7** ($[Th(IV)]_{tot}$ = 116 mM, pH_C 3.05, 44% pentamers, Fig. 2, bottom). For the latter two samples the first oxygen shell splitting due to bridging $–OH^–$ and terminal $–OH^–/–OH_2$ requires inclusion of two separate oxygen paths to satisfactorily reproduce the measurements. The increasing N_{Th} values found for these samples reflect the increasing percentage of pentamers observed by ESI MS. From the species distribution of **A3** one would expect N_{Th} = 0.6 due to 28% dimers (N_{Th} = 1) and 35% pentamers (N_{Th} = 2.4). Sample **A7** should have N_{Th} = 1.37 from 31% dimers and 44% pentamers. Measured values are N_{Th} = 0.3 and N_{Th} = 0.9 for **A3** and **A7**, respectively. The somewhat lower N_{Th} values might be due to the simultaneous presence of different Th(IV) polymers with a certain spread of Th–Th second next neighbor distances: as we have previously shown for Zr(IV),[12] Th (IV)[28] and Pu(IV)[33] oligomers, the destructive interference can even lead to complete extinction of the metal–metal backscattering signal in the EXAFS of oxy/hydroxide polymers and colloids. The coordination numbers N_{Th} of **D2**, 1.06(theo) *vs.* 1.7, **C1** 1.5(theo) *vs.* 1.8 and **B1** 1.9(theo) *vs.* 3.1 match reasonably well. Note the general trend that with increasing percentage of Th(IV) present as polymeric species the overall EXAFS amplitude (corresponding to the dominant FT magnitude peak height at ~1.9 Å) is strongly diminished compared to the monomeric aquo or hydroxo species.

At first glance, the EXAFS signatures obtained in this study for samples dominated by Th(IV) pentamers appear similar to data presented for suspended oxy/hydroxide colloids and an amorphous solid phase designated as $Th(OH)_4(am)/ThO_n(OH)_{4-2n}{\cdot}xH_2O(am)$ in ref. 28. However, the species described in the earlier study exhibit a much broader first shell Th–O pair distribution (~2.45–3.15 Å), longer Th–Th distance (approaching 4 Å) and generally reduced second next neighbour metal visibility as expected for amorphous oxy/hydroxides. In contrast to that, the present EXAFS metrical parameters are in accordance with the assumption of well ordered entities.

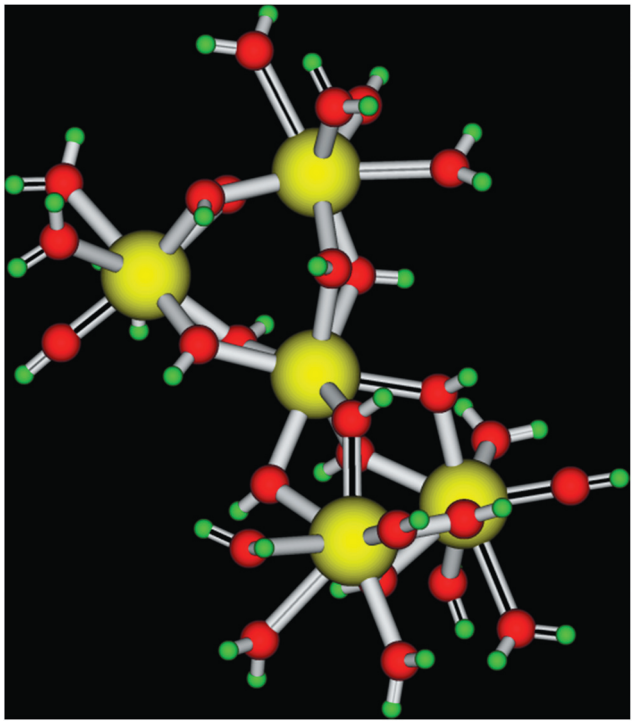

Fig. 3 Th pentamer composed of two dimers linked by an additional monomer.

Table 2 Th L3-EXAFS least-squares fit parameters

ID	Fit-range (Å)	Shell	N	R (Å)	σ^2 (Å^2)	ΔE_0 (eV)	R-factor
A1	1.53–2.24	O	8.8	2.45	0.0043	5.03	0.0110
A2	1.44–2.27	O	9.3	2.47	0.0049	6.17	0.0026
A3	1.41–4.11	O(1)	8.2	2.44	0.0071	5.75[a]	0.0190
		O(2)	1.1	2.49	0.0027	5.75[a]	
		Th	0.3	3.95	0.0001	7.85	
A7	1.50–4.11	O(1)	6.5	2.43	0.0067	4.39[a]	0.0161
		O(2)	1.9	2.48	0.0051	4.39[a]	
		Th	0.9	3.92	0.0032	6.71	
B1	1.50–4.14	O	8.8	2.49	0.0129	8.76	0.0270
		Th	3.1	3.94	0.0099	3.07	
C1	1.47–4.17	O(1)	7.9	2.43	0.0108	6.48[a]	0.0318
		O(2)	1.6	2.57	0.0108	6.48[a]	
		Th	1.8	3.94	0.0044	8.12	
D2	1.56–4.11	O(1)	3.8	2.40	0.0020[a]	8.94[a]	0.0275
		O(2)	3.4	2.55	0.0020[a]	8.94[a]	
		Th	1.7	3.87	0.0061	5.24	

EXAFS least-squares fit results, $S_0^2 = 1.0$ (errors in N: ±0.5; errors in R: ±0.02 Å).[a] Indicates global parameter for both oxygen shells.

While reliable data for the first two coordination shells (oxygen and second shell thorium atoms) are easily derived from XAFS spectra, information on the higher shells is hard to obtain by this method. Of particular interest in the present study is the second next Th–Th distance. Hence, high energy X-ray scattering (HEXS)[34,35] was performed on the solutions of series **A** at the Advanced Photon Source sector 11 beamline (see Experimental). Samples **A1**–**A7** were measured by ESI MS, shipped to the APS and measured there *ca.* 14 days after preparation. By repeatedly measuring the species distribution by ESI MS the stability of the pentamers was assured. Only a slight increase of the dimer fraction is visible (Table 1). Peak assignments of the pair distribution functions (PDF) are made by comparing peak positions from the hydrolyzed solution with those previously obtained from a Th dihydroxo-bridged dimer.[3] For sample **A7**, *e.g.*, the correlation at 2.48(10) Å is assigned to 9.3(3) oxygen atoms arising from either Th–water or Th–hydroxide interactions in accordance with Th–O distances obtained by XAFS. A peak at 3.12(8) Å is attributed to the corresponding H atoms from the Th-bound waters.[36] A correlation at 3.9 Å results from 1.1(2) Th–Th interactions, in excellent agreement with the XAFS data (Table 2). Second coordination sphere waters give rise to a broad peak at about 4.5–5.5 Å, with possibly some chloride ion contribution. With increasing Th concentration a distinct longer ranged correlation at >6.7 Å is detected, indicative of the presence of oligomers larger than the dimer. A HEXS derived PDF for sample **A7** is provided as ESI.†

Since the Th–Th and Th–O distances alone cannot unambiguously solve the geometrical structure of the pentamer, gas-phase quantum chemical calculations were used to investigate various possible structures. The resulting Th–O and Th–Th distances were compared with the experimental data. Considering a square-planar structure for the tetramer and an octahedral structure for the hexamer, an obvious candidate for the pentamer structure is the square-pyramid. The set of considered pentamers thus includes square-pyramidal structures with differing bridges, as well as a complex with two dimers, each bridged by four OH-groups to a central Th(IV), labeled dimer–monomer–dimer (DMD), and a DMD-derived structure where the dimer bonds are broken and four monomers are binding to the central Th(IV) (labeled five monomers, 5M). Visualizations of these structures can be found as ESI.† We tried to further refine the various optimized structures by including the effects of 'proton hopping' between water, oxo- and OH-groups by moving protons to various possible locations. As no treatment of solvent effects was included in the calculations, relative energies cannot be considered reliable, while the Th–O bond distances will be typically overestimated by several pm.

Th–O and Th–Th distances for the investigated complexes are given in Table 3. The Th–O distances scatter over a rather wide range due to the different groups and their coordination in the complexes. On the other hand, the Th–Th distances provide a clear basis to discriminate unlikely structures in comparison to the experimental data. For all pyramidal structures we find Th–Th distances in the pyramidal base strongly deviating from experimental values, especially the distance between two non-bridged (second next neighbor) Th(IV) cations cannot be confirmed by experimental observations. The same holds for the 5M-structure with four monomers bridging to a central Th(IV), where a Th–Th distance between two outer units is found at 541 pm. The only structure in agreement with the long Th–Th correlation obtained by HEXS data is obtained for the DMD complex (Fig. 3), for which no Th–Th distances are obtained in the 500–600 pm range. None of the other complexes exhibit Th–Th distances longer than 600 pm. Due to the deviations from experimental Th–O bond distances and the uncertainties of the torsion-angle between the two dimer subunits, the calculated Th–Th distances of 714 and 770 pm are subject to relatively

Table 3 Th–O distances for various complexes. All distances are given in pm. The different types of oxygen are distinguished as OH_{bridge}, O_{bridge}, OH_{lig} and H_2O_{lig} as obtained from geometry optimization at the RI-DFT BP-86 level. The best agreement with structural data from HEXS and XAFS was obtained for the species presented in italic font

Complex	Method	Th–Th	Th–O (OH_{bridge})	Th–O (O_{bridge})	Th–O (OH_{lig})	Th–O (H_2O_{lig})
$Th_5O_4(OH)_8(H_2O)_{16}^{4+}$ (pyramidal)	BP-86	377[a] 391, 552[b]	236–240	230–233	218	263–278
$Th_5O_8(H_2O)_{20}^{4+}$ (pyramidal)	BP-86	377[a] 366, 517[b]	—	220–237	—	265–272
$Th_5(OH)_{16}(H_2O)_{12}^{4+}$ (pyramidal)	BP-86	432[a] 422, 596[b]	237–263	—	213	251–260
$Th_5O_5(OH)_8(H_2O)_{16}^{2+}$ (pyramidal)	BP-86	361[a] 367, 519[b]	238	257–259[e] 228, 246	226	258, 266, 285
$Th_5(OH)_{16}(H_2O)_{12}^{4+}$ (DMD)	*BP-86*	*397–401* *714–770*	*237–248*	—	*212–214*	*264–271*
$Th_5(OH)_{16}(H_2O)_{16}^{4+}$ (5M)	BP-86	384, 541	244[c] 229[d]	—	235	166–267

[a] Top–base. [b] Base–base. [c] Central. [d] Outer. [e] O_{base}.

large errors. A treatment of solvent effects on the structure should reduce these errors. Nevertheless, the present accuracy is sufficient for our purpose to consider the DMD-complex as a realistic model for the pentamer structure.

Conclusions

From the results presented above we conclude that the Th(IV) pentamer is formed by two dimers linked by a central Th(IV) cation through hydroxide bridges (Fig. 3). The fact that only one Th–Th distance at ~3.9 Å is obtained by XAFS eliminates all pyramidal structures suggested by quantum chemical calculations. In this case, split and shorter Th–Th distances should have been observed. Furthermore, the second Th–Th interaction would be much shorter than 6.7 Å observed by HEXS. The presence of oxygen- instead of hydroxide-bridges cannot be excluded from ESI MS data alone as discussed in ref. 12. Likewise, the presence of oxo- in addition to hydroxo-bridges would not be unambiguously detected by EXAFS due to Th–O shell splitting caused by terminal H_2O. On the other hand, the dimer described in ref. 3 is formed by hydroxide bridges and, in contrast to Pu(IV),[2] freshly formed thorium polymer is well known to preferentially undergo olation.[37,38] These findings are also corroborated by the quantum chemical cluster calculations considering 'proton hopping'.

From a mechanistic point of view the formation of pentamers of this structure is also plausible. Dimers and monomers are the dominating species in slightly more undersaturated solutions. Formation of more compact species such as the pyramidal pentamer should be preceded by formation of trimers and tetramers which are at no time observed by ESI MS in appreciable amounts (in contrast to polymerization in perchloric acid at high ionic strength[4]). In the present case of low ionic strength in hydrochloric acid, linkage of dimers by monomers seems to be energetically favourable over stepwise size increase or over formation of tetramers from two dimers. A second important fact is that these polymers are subject to continuous hydrolysis, *i.e.*, the number of OH^- ligands of the complex is not fixed by coordination but increases with increasing pH. This suggests the presence of a stable backbone formed by the central atom and the eight hydroxide bridges. The outer thorium ions form a partly hydrolyzed hydration shell where the degree of protolysis and hence the total number of hydroxide ligands of the polymer depend on the pH.

Acknowledgements

We acknowledge the use of the APS Sector 1 and thank L. Soderholm, S. Skanthakumar, and R. E. Wilson for help with the HEXS measurements and valuable discussions. The KIT synchrotron source ANKA is acknowledged for providing beamtime. We thank Sebastian Büchner for assistance with the ESI MS measurements.

References

1 M. Henry, J. P. Jolivet and J. Livage, *Struct. Bonding*, 1992, **77**, 153–206.
2 L. Soderholm, P. M. Almond, S. Skanthakumar, R. E. Wilson and P. C. Burns, *Angew. Chem., Int. Ed.*, 2008, **47**, 298–302.
3 R. E. Wilson, S. Skanthakumar, G. Sigmon, P. C. Burns and L. Soderholm, *Inorg. Chem.*, 2007, **46**, 2368–2372.
4 N. Torapava, I. Persson, L. Eriksson and D. Lundberg, *Inorg. Chem.*, 2009, **48**, 11712–11723.
5 M. Wickleder, B. Fourest and P. Dorhout, in *The Chemistry of Actinide and Transactinide Elements*, ed. L. R. Morss, N. M. Edelstein, J. Fuger and J. J. Katz, Springer, Heidelberg, 2006, vol. 1, pp. 117–129.
6 V. Neck, R. Müller, M. Bouby, M. Altmaier, J. Rothe, M. A. Denecke and J. I. Kim, *Radiochim. Acta*, 2002, **90**, 485–494.
7 M. H. Rand, J. Fuger, I. Grenthe, V. Neck and D. Rai, *Chemical Thermodynamics of Thorium*, Elsevier, North-Holland, Amsterdam, 2009.
8 M. Wilm and M. Mann, *Anal. Chem.*, 1996, **68**, 1–8.
9 J. B. Fenn, *J. Biomol. Tech.*, 2002, **13**, 101–118.
10 R. B. Cole, *Electrospray Ionization Mass Spectrometry*, John Wiley and Sons, New York, 1997.
11 C. Walther, M. Fuss and S. Büchner, *Radiochim. Acta*, 2008, **96**, 411–425.
12 C. Walther, J. Rothe, M. Fuss, S. Büchner, S. Koltsov and T. Bergmann, *Anal. Bioanal. Chem.*, 2007, **388**, 409–431.
13 C. Moulin, B. Amekraz, S. Hubert and V. Moulin, *Anal. Chim. Acta*, 2001, **441**, 269–279.
14 C. Walther, M. Fuss, S. Büchner and H. Geckeis, *J. Radioanal. Nucl. Chem.*, 2009, **282**, 1003–1008.
15 *TURBOMOLE, V6.3 2011, a development of University of Karlsruhe and Forschungszentrum Karlsruhe GmbH, 1989–2007*, TURBOMOLE GmbH, since 2007; available from http://www.turbomole.com

16 K. Eichkorn, O. Treutler, H. Ohm, M. Haser and R. Ahlrichs, *Chem. Phys. Lett.*, 1995, **242**, 652–660.
17 K. Eichkorn, O. Treutler, H. Ohm, M. Haser and R. Ahlrichs, *Chem. Phys. Lett.*, 1995, **240**, 283–289.
18 K. Eichkorn, F. Weigend, O. Treutler and R. Ahlrichs, *Theor. Chem. Acc.*, 1997, **97**, 119–124.
19 S. H. Vosko, L. Wilk and M. Nusair, *Can. J. Phys.*, 1980, **58**, 1200–1211.
20 P. A. M. Dirac, *Proc. R. Soc. London, Ser. A*, 1929, **123**, 714–731.
21 J. C. Slater, *Phys. Rev.*, 1951, **81**, 385–390.
22 J. P. Perdew, *Phys. Rev. B*, 1986, **33**, 8822–8824.
23 A. D. Becke, *Phys. Rev. A: At., Mol., Opt. Phys.*, 1988, **38**, 3098–3100.
24 X. Y. Cao, M. Dolg and H. Stoll, *J. Chem. Phys.*, 2003, **118**, 487–496.
25 X. Y. Cao and M. Dolg, *THEOCHEM*, 2004, **673**, 203–209.
26 K. Dardenne, B. Brendebach, M. A. Denecke, X. Liu, J. Rothe and T. Vitova, *J. Phys.: Conf. Ser.*, 2009, **190**, 012037.
27 J. Vandenborre, A. Abdelouas and B. Grambow, *Radiochim. Acta*, 2008, **96**, 515–520.
28 J. Rothe, M. A. Denecke, V. Neck, R. Müller and J. I. Kim, *Inorg. Chem.*, 2002, **41**, 249–258.
29 W.-C. Wang and C. Yu, *Phys. Status Solidi A*, 1998, **168**, 351.
30 C. Hennig, *Phys. Rev. B: Condens. Matter Mater. Phys.*, 2007, **75**, 035120–035127.
31 R. E. Wilson, S. Skanthakumar, P. C. Burns and L. Soderholm, *Angew. Chem., Int. Ed.*, 2007, **46**, 8043–8045.
32 E. D. Crozier, *Phys. B*, 1995, **208&209**, 330–333.
33 C. Walther, J. Rothe, B. Brendebach, M. Fuss, M. Altmaier, C. M. Marquardt, S. Büchner, H.-R. Cho and J.-I. Yun, *Radiochim. Acta*, 2009, **97**, 199–207.
34 S. Skanthakumar and and L. Soderholm, Actinides 2005-Basic Science, Applications and Technology, 2006, **893**, 411–416.
35 L. Soderholm, S. Skanthakumar and J. Neuefeind, *Anal. Bioanal. Chem.*, 2005, **383**, 48–55.
36 S. Skanthakumar, M. R. Antonio, R. E. Wilson and L. Soderholm, *Inorg. Chem.*, 2007, **46**, 3485–3491.
37 L. G. Sillen, Symposium on Co-ordination Chemistry, Copenhagen, 1953.
38 G. L. Johnson and L. M. Toth, *Plutonium(IV) and Thorium(IV) Hydrous Polymer Chemistry TM-6365*, Oak Ridge National Laboratory, Tennessee, 1978.
39 B. I. Nabivanets and L. N. Kudritskaya, *Ukr. Khim. Zh. (Russ. Ed.)*, 1964, **30**, 891.
40 J. L. Ryan and D. Rai, *Inorg. Chem.*, 1987, **26**, 4140–4142.
41 D. Rai, D. A. Moore, C. S. Oakes and M. Yui, *Radiochim. Acta*, 2000, **88**, 297–306.